2008-3735

38th Fluid Dynamics Conference and Exhibit, 23–26 June 2008, Seattle, Washington

Starting Issues and Forward-Facing Cavity Resonance in a Hypersonic Quiet Tunnel

Thomas J. Juliano *

School of Aeronautics and Astronautics, Purdue University, West Lafayette, IN 47907-1282

Rodrigo Segura †

Institute of Fluid Mechanics and Aerodynamics, Universität der Bundeswehr München

85579 Neubiberg, Germany

Matthew P. Borg *

Katya Casper *

Michael J. Hannon, Jr. †

Brad M. Wheaton *

and Steven P. Schneider ‡

School of Aeronautics and Astronautics, Purdue University, West Lafayette, IN 47907-1282

Blunt 70° sphere-cones with a 2.5-in. diameter were successfully started in the Boeing/AFOSR Mach-6 Quiet Tunnel when the flow was quiet and the nozzle-wall boundary layer was laminar. However, under noisy flow with thicker turbulent boundary layers, similar models with a 2.0-in. diameter barely started. A porous Apollo capsule with a 2.0-in. diameter at 24° angle of attack failed to start. In an effort to start larger models with stronger bow shocks, new sting-support and diffuser sections were installed. Downstream of the nozzle exit, the diameter was increased from 9.5 to 14.1 in. A series of inserts are being installed behind the backward-facing step in attempts to control the shock/boundary-layer interactions induced by models. These efforts have not yet been successful. During this time, the maximum stagnation pressure for quiet flow has typically ranged from 120 to 145 psia. Pressure measurements near the exit of the Mach-6 diffuser indicated that quiet flow may extend far downstream under some circumstances. A laser differential interferometer was rebuilt for the Mach-6 tunnel with an improved signal-to-noise ratio. Quiet-flow experiments were also carried out at Mach 4 with a pressure transducer at the base of a forward-facing cavity. Computational predictions of self-resonance in deep cavities were confirmed experimentally. For moderately deep cavities, small freestream disturbances were amplified even under quiet flow.

Nomenclature

D	forward-facing cavity diameter
k	roughness height
L	forward-facing cavity length
M	Mach number

*Research Assistant. Student Member, AIAA.

†Research Assistant.

‡Professor. Associate Fellow, AIAA.

p pressure
t time
z axial tunnel coordinate, $z = 0$ at throat
δ bow-shock standoff distance
λ laser wavelength

Subscripts
i initial
0 stagnation

I. Introduction

I.A. Hypersonic Laminar-Turbulent Transition

Understanding laminar-turbulent transition in hypersonic boundary layers is important for prediction and control of heat transfer, skin friction, and other boundary layer properties. Vehicles that spend extended periods at hypersonic speeds may be critically affected by the uncertainties in transition prediction, depending on Reynolds number. Although slender vehicles are the primary concern, blunt vehicles are also affected by transition.[1] However, the mechanisms leading to transition are still poorly understood, even in low-noise environments.

Many transition experiments have been carried out in conventional ground-testing facilities over the past 50 years.[2] However, these experiments are contaminated by the high levels of noise that radiate from the turbulent boundary layers normally present on the wind tunnel walls.[3] Noise level is taken here as the root-mean-square pitot pressure ($\tilde{p}$) divided by mean pitot pressure ($\bar{p}$). These noise levels, typically 0.5–1%, are an order of magnitude larger than those observed in flight.[4,5] These high noise levels can cause transition to occur an order of magnitude earlier than in flight.[3,5] In addition, the mechanisms of transition operational in small-disturbance environments can be changed or bypassed altogether in high-noise environments; these changes in the mechanisms change the parametric trends in transition.[4] Mechanism-based prediction methods must be developed, supported in part with measurements of the mechanisms in quiet wind tunnels.

I.B. Development of Quiet-Flow Wind Tunnels

Only in the last two decades have low-noise supersonic wind tunnels been developed.[3,6] This development has been difficult, since the test-section wall boundary layers must be kept laminar in order to avoid high levels of eddy-Mach-wave acoustic radiation from the normally-present turbulent boundary layers. A Mach-3.5 tunnel was the first to be successfully developed at NASA Langley.[7] Langley then developed a Mach-6 quiet nozzle, which was used as a starting point for the new Purdue nozzle.[8] It was removed from service due to operational conflicts and changing research priorities. The facility is now housed at Texas A&M. The Boeing/AFOSR Mach-6 Quiet Tunnel (BAM6QT) is the first operational hypersonic quiet tunnel with low operating costs and good optical access.[9]

I.C. The Boeing/AFOSR Mach-6 Quiet Tunnel

Design of the BAM6QT began in 1996. From the outset, the tunnel had two goals: run with a low noise level and do so affordably. The target was to achieve quiet flow for stagnation pressures up to 150 psia (1000 kPa). This corresponds to a unit Reynolds number of $3.4 \cdot 10^6$/ft. ($11 \cdot 10^6$/m) for a stagnation temperature of 433 K at Mach 6. Quiet facilities require low levels of noise in the inviscid flow entering the nozzle through the throat, and laminar boundary layers on the nozzle walls.[10,11] Many of the characteristics of the Langley quiet tunnels were employed. For example, the BAM6QT incorporates boundary layer suction before the throat and the nozzle features a long, straight-walled section to delay the onset of Görtler vortices.[12] The first 0.76 m of the nozzle features an electroformed nickel finish, which has no seams and can be highly polished with minimal roughness and waviness.[13]

In order to have a low operating cost, a Ludwieg tube design was chosen over the blowdown configuration (Figure 1). A Ludwieg tube is a pipe with a converging/diverging nozzle on the end. The Ludwieg tube is

operated through many cycles of expansion-wave reflection within the driver tube, providing a run time of a few seconds, during which the Reynolds number falls quasi-statically. Modern instrumentation makes this moderately short run time more than sufficient for measurements of instability and transition. Compared to a blow-down tunnel, the run-time and air-supply costs are reduced by one or two orders of magnitude. The complex and costly settling chamber is eliminated, and the necessary high-quality air filtering is carried out during the slow charging of the driver tube, which is maintained as a clean room. For the BAM6QT, the run time is currently about 4 or 5 seconds, whereas the tunnels at NASA Langley typically ran for up to 60 minutes and could run continuously.[3]

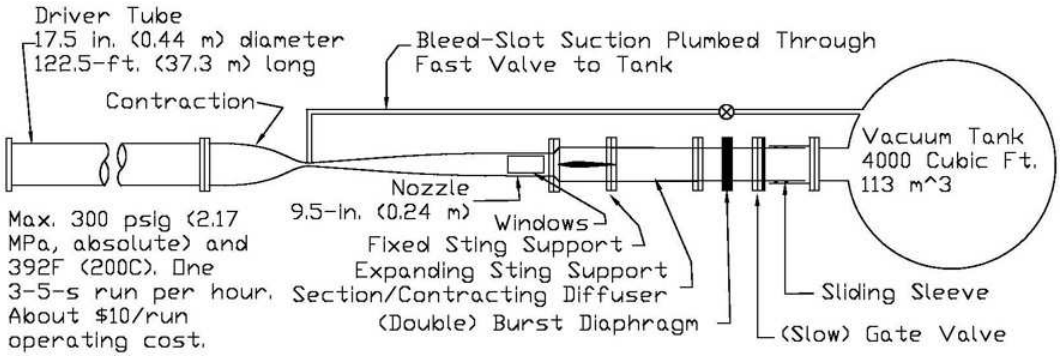

Figure 1: Schematic of Boeing/AFOSR Mach-6 Quiet Tunnel

Figure 2 shows Section 8, the last nozzle section. The region of useful quiet flow lies between the characteristics marking the onset of uniform flow and the characteristics marking the upstream boundary of acoustic radiation from the onset of turbulence in the nozzle-wall boundary layer. A 7.5° sharp cone is drawn on the figure. The rectangles are drawn on the nozzle at the location of window openings, all but one of which are presently filled with blank metal inserts.

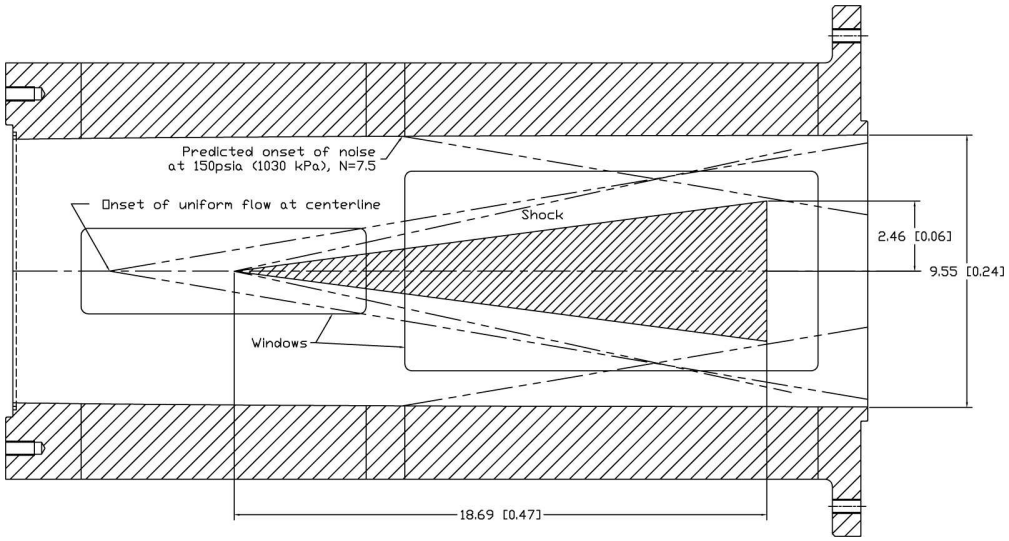

Figure 2: Schematic of Mach-6 quiet nozzle with 7.5° cone model. Dimensions are inches [meters].

II. Status of Tunnel Quiet-Flow Performance

Tunnel performance from February 2005 through December 2006 is reported in Reference 14. Performance from January to April 2007 is reported in Ref. 15, and from May through December 2007 in Ref. 16.

From January through April 2008, the BAM6QT exhibited several changes in its quiet performance. These changes are in addition to the changes in run time and separation as a result of the new sting-support section, discussed below. The quiet performance is mostly dependent upon the state of the nozzle from the

bleed lip to the origin of the Mach lines at the end of the test section (e.g., on scratches or dust on the nozzle wall). It is therefore expected that the quiet performance is largely decoupled from the changes in the sting-support section.

The electroformed nickel nozzle has been installed in the tunnel since it was repolished in September 2007. The tunnel began the year running quietly below $p_0 \approx 140$ psia. In late February, the tunnel was accidentally run without opening the gate valve between the double diaphragms and the vacuum tank. This resulted in a shock traveling upstream back into the nozzle. The first few runs immediately afterward, with a starting pressure of 120 psia, showed no quiet flow. Performance improved after more runs, and two weeks after the accident the quiet pressure was reliably 143 psia.

At that time, quiet runs at higher pressure exhibited many more turbulent bursts than quiet runs at lower pressure (150–200 bursts per second during the quiet portion after starting at 150 psia, 80 per second when starting at 130 psia, 25 per second when starting at 110 psia, and 5 per second when starting at 90 psia). It is curious that a large number of turbulent bursts occurs within an overall laminar flow under these conditions.

This increase in turbulent bursts is similar to the behavior encountered when a similar, accidental gate-valve-closed run was made in March 2007. In both cases, continued tunnel runs have resulted in a decrease in the quantity of turbulent bursts. This improvement could be because dust dislodged or pushed upstream by the shock in the nozzle is gradually being blown out of the nozzle. Typically, clean preheat air was run through the NASA Langley quiet tunnels for several minutes before each run, which helped to clear out dust. This is not an option for the BAM6QT because its runs only last for a few seconds.

In early April 2008, a run that began quiet at 137 psia spontaneously became noisy during the run. Subsequent testing identified that the new maximum quiet pressure was 89 psia. Suspecting that the decrease was due to dust in the nozzle, a very-high-pressure ($p_{0i} = 251$ psia) run was conducted in an effort to blow it out. The quiet pressure increased to 105 psia, still less than the target of 150 psia.

In May 2008 the nozzle was opened in order to use acetone and Kimwipes to clean dust out of the nozzle and inspect it for scratches. No scratches were found. After the nozzle was reattached, three high-pressure runs were conducted. The maximum stagnation quiet pressure was subsequently found to be 130 psia, with about 20 turbulent bursts per second.

While the nozzle was opened, its interior was photographed looking upstream from $z = 0.76$ m downstream of the throat, with a pattern of intersecting radial lines placed outside the far end of the nozzle (Figure 3). This method of nozzle inspection was recommended by Steve Wilkinson, who used it to examine waviness in the alternate axisymmetric nozzle of the NASA Langley Mach 3.5 Quiet Tunnel. The method does not work as well for the Mach 6 nozzle because of its small throat and long length — no light reflected from the aft half of this nozzle portion towards the camera. The upstream nozzle section features a seamless, electroformed layer of nickel. No azimuthal defects are evident, but several bands with different reflections are visible normal to the tunnel axis. It is very difficult to interpret these results.

Figure 3: Photograph of Mach 6 nozzle looking upstream towards the throat showing some waviness

III. Description of New Sting Support Section and Inserts

Ref. 15 describes the difficulties starting blunt models in the BAM6QT, and the new sting-support section that was designed to improve starting. The new section has a larger diameter so that the shock from the blunt model impinges on the free shear layer downstream of the expansion fan, with the idea that the favorable pressure gradient will inhibit separation from spreading upstream (Figure 4).

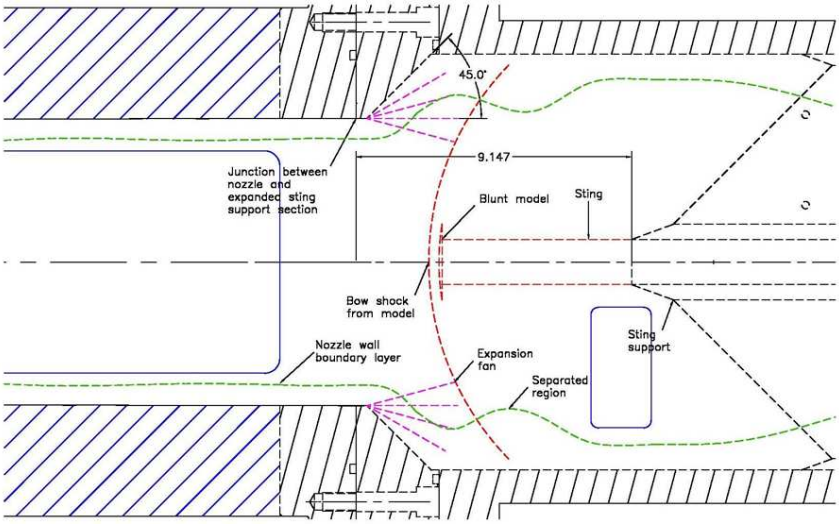

Figure 4: Expected flow features of new, larger-diameter sting support section

Instead of holding a constant inner diameter of 9.5 in., as with the old sting-support section, the new approach has an adapter flange attached at the end of the nozzle, with a 45° expansion to an inner diameter of 14.125 in. This 14.125-in. inner diameter is held constant through the 3-ft. sting-support section until reaching the new diffuser section. The diffuser section then has a contracting taper of approximately 0.9° through most of its length, reaching an inner diameter of 12 in. at the downstream end (Figure 5). This allows a connection to the remaining downstream sections of the original tunnel configuration.

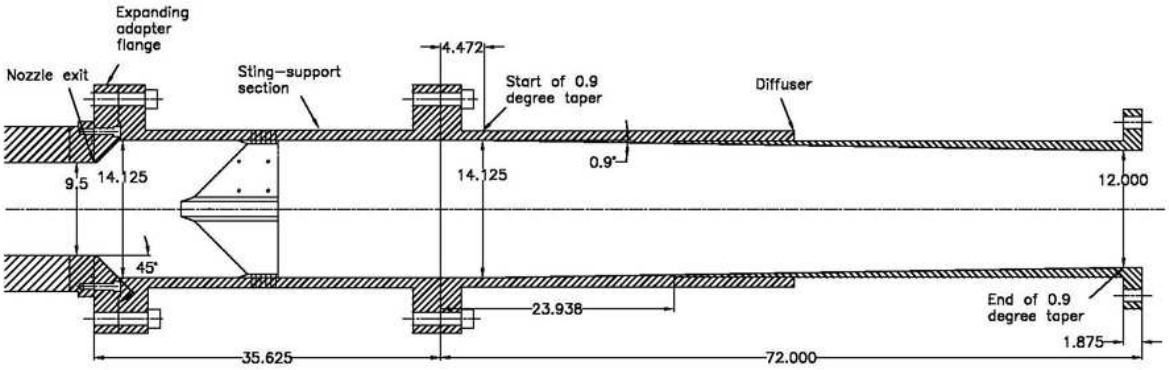

Figure 5: Schematic of modified sting-support and diffuser sections with test section. Dimensions in inches.

The original plan for the new diffuser included inserts to provide a more gradual expansion and recompression downstream of the nozzle. Figure 6 is a schematic of a 9° nylon insert that is placed on top of the expansion ramp. By decreasing the turning angle the flow should be less prone to separate.

Figure 7 is a schematic of a straight-pipe insert made of stainless steel. This insert provides a slot between the downstream end of the nozzle and the insert. The slot width may vary from 0 to 1.5 in. The pressure on the outside of the pipe insert is expected to be lower than the main flow pressure. The suction from this pressure difference would then remove much of the upstream boundary layer, again promoting attached flow. The initial performance of these inserts is described in the next section. Also, a porous straight-pipe insert is planned but is yet to be built.

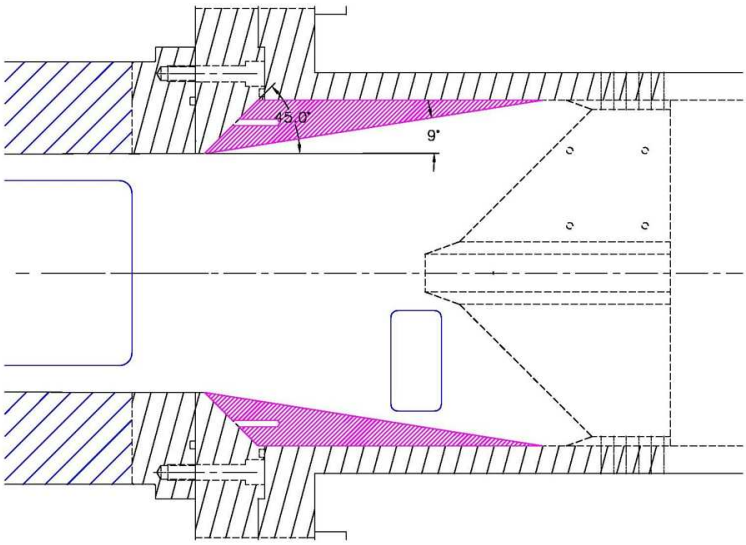

Figure 6: Schematic of 9° nylon insert in new sting-support section

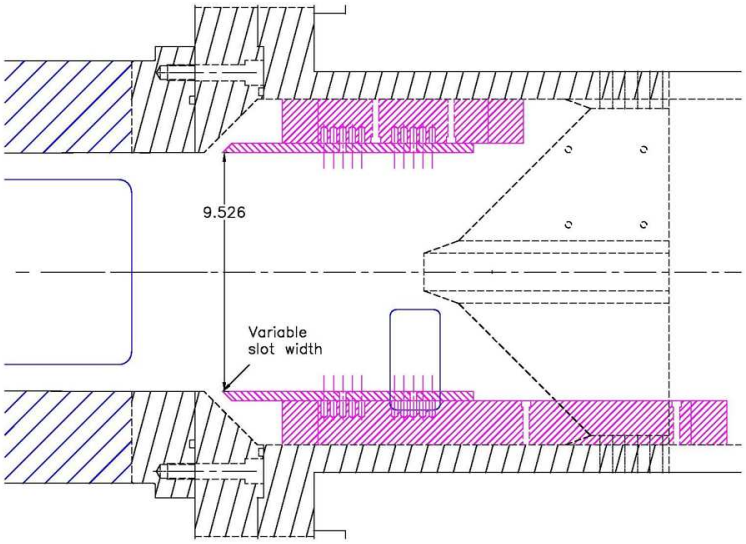

Figure 7: Schematic of steel straight-pipe insert in new sting-support section. Dimensions in inches.

IV. Performance of New Sting Support Section

Tests were performed from March to October 2007 to determine the starting capabilities of the original tunnel sting-support section and diffuser using a 70° half-angle sphere cone with variable base diameter in 0.25-in. increments. For quiet flow, these tests indicated a maximum starting diameter of 2.5 in. In noisy flow, the 2-in.-diameter model only started in about 15% of the tests, but they were not repeatable. This result was surprising since it was expected that larger models could start with turbulent nozzle-wall boundary layers, which are less prone to separation.

Tests with this model in the new sting-support section in December 2007 found no improvement in the maximum starting model size in quiet or noisy flow. When the model was far forward ($z = 2.33$ m), the starting performance was the same as the original configuration. When it was farther back ($z = 2.65$ m), the smallest model tested (2 in. diameter) would not start. This is contrary to the concept for the larger diameter section. The run time of the modified tunnel setup decreased to approximately half that of the original tunnel configuration and the noise level measured by a pressure transducer on the front surface of the blunt model doubled. Additional discussion of these results is available in Ref. 17.

IV.A. No Insert — 45° Expansion Corner

Tunnel runs with the new diffuser section and no insert were conducted in February 2008 with an isolated roughness on the nozzle wall. There was no model or sting installed in the tunnel, although the sting support struts were installed. Two hot films on the nozzle wall were used to take boundary-layer measurements. The hot films were located at tunnel coordinates $z = 1.89$ m (74.25 in.) and $z = 2.07$ m (81.50 in.) on the bottom of the test section. The roughness was located at $z = 1.92$ m (75.75 in.) on the upstream side window insert. The roughness height k was small compared to the test-section diameter and the hot films were offset 90° from the roughness element. The roughness was not expected to affect the boundary layer near the hot films and, no effect of roughness height on those hot films was detected.

Several runs were conducted at an initial stagnation pressure of 120 psia. At this pressure, disturbances appeared during startup and the first second of the run, followed by around 2.5 s of normal quiet flow as in Figure 8. The disturbances often took the form of several large spikes made up of smaller 100 Hz oscillations and were prevalent mostly on the downstream hot film. Figure 8b shows an expanded view of the hot-film traces during tunnel start-up. Both hot films exhibit the large spikes in voltage, but the downstream hot film signal contains smaller 100 Hz spikes while the upstream hot film does not, except before $t = 0.35$ s.

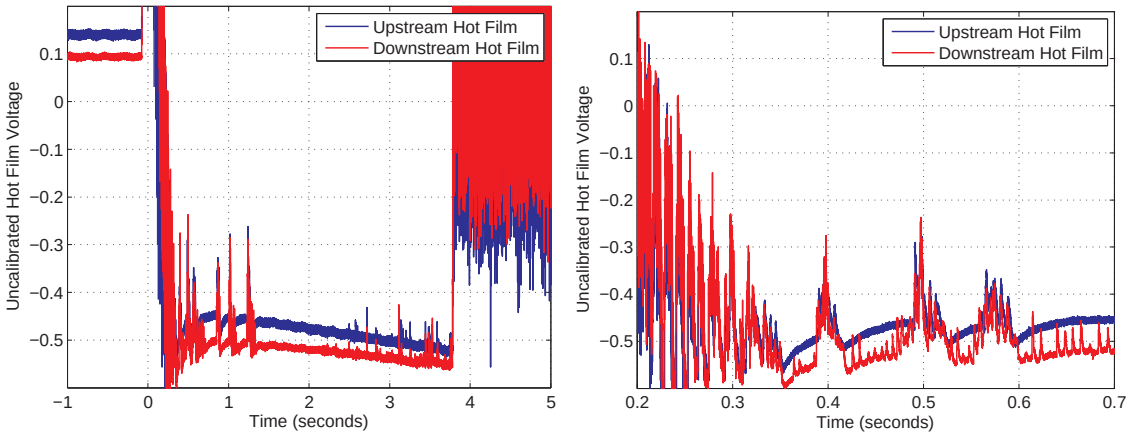

(a) Entire run

(b) Magnified view showing startup disturbance

Figure 8: Empty tunnel, $p_{0i} = 120.4$ psia, $p_{vacuum} = 1.65$ torr, $k = 0.76$ in.

When running at an initial stagnation pressure range of 135–140 psia, the hot film signals were dominated by the same 100 Hz disturbance throughout the entire run (Figure 9). The spikes were characterized by a sharp increase in hot film voltage followed by a smoother drop-off. While normal turbulent bursts last on the order of 1.5 ms,[14] these spikes last an order of magnitude longer (0.01 s), as shown in Figure 9b. This suggests that the disturbances are not turbulent bursts.

At 90 psia stagnation pressure, the disturbances again appeared, more often on the downstream hot film than the upstream hot film. For some runs, the spikes only occurred during the first 0.5 s of the run and then disappeared, similar to the previously discussed runs at 120 psia. During other runs at 90 psia, the disturbances were dominant during the entire run, as in Figure 10. Though all runs at 90 psia had similar initial conditions, the appearance of the 100 Hz disturbance during the entire run (as opposed to only during startup) was unpredictable.

When running the tunnel empty and without inserts in the diffuser section, the 100 Hz disturbance tended to dominate the runs at 135–140 psia. At 120 psia, the disturbance tended to happen only during startup and the first 0.5–1 seconds of the run. At 90 psia, the spikes either dominated the flow during the entire run or disappeared after 0.5 s in an unpredictable manner. The spikes were more often visible in the downstream hot film (closer to the diffuser section), suggesting that the disturbances originate downstream and travel upstream within the subsonic part of the boundary layer.

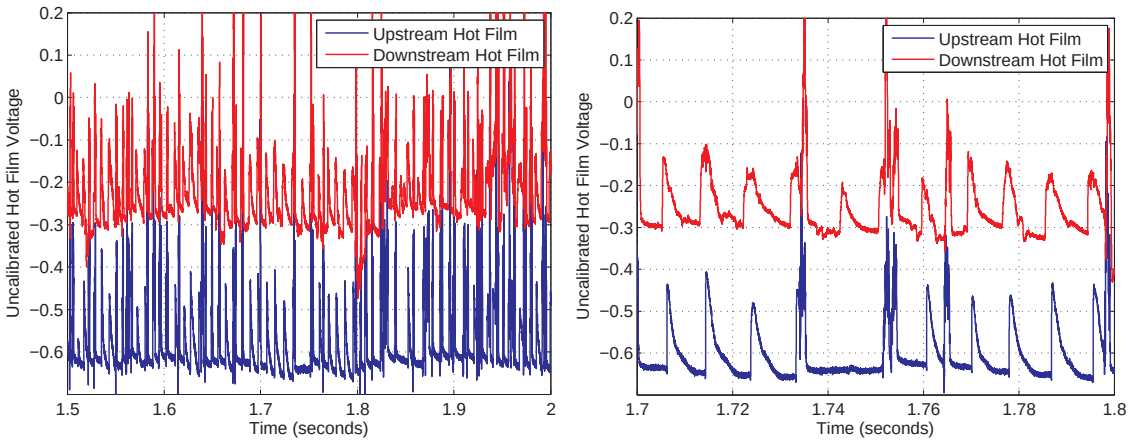

Figure 9: Close-up views of 100 Hz disturbance. Empty tunnel, $p_0 = 140.9$ psia, $p_{vacuum} = 1.89$ torr, $k = 0.26$ in.

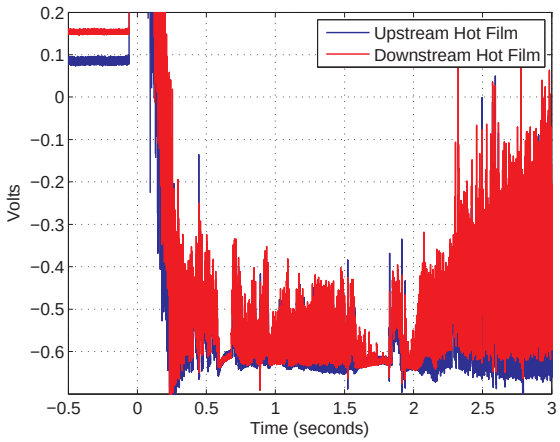

Figure 10: View of 100 Hz disturbance dominating a run. Empty tunnel, $p_0 = 90.4$ psia, $p_{vacuum} = 1.81$ torr, $k = 0.38$ in.

IV.B. Nylon Insert — 9° Expansion Corner

IV.B.1. Sharp Cone

In early March 2008, the nylon insert with a 9° taper was installed in the sting-support section. The first runs with the new insert were conducted with a 4 in.-base-diameter, 7° half-angle sharp cone at zero angle of attack. The tip was located 1.96 m downstream of the throat. The initial stagnation pressure was 90.0 ± 0.5 psia and the bleed line was closed because a conventional noise level was desired. Measurements of tunnel noise level and separation were made by two wall-mounted hot films.

Figure 11 shows typical results from this series of tests. The lower trace is the upstream hot film, located 1.89 m downstream of the throat. The upper trace is the downstream hot film at 2.07 m. The run begins at $t = 0.0$ s and runs noisy, as expected, until $t = 4.6$ s. The next 0.8 s shows very large fluctuations. Then the upstream hot film returns to its original level, whereas the downstream hot film jumps to a higher level. Previous work has shown that an increase in the mean level of the hot-film output is an indicator of a separated boundary layer.[18] After another 1.5 s, the upstream hot film again shows large fluctuations. At $t = 8.0$ s, both voltages again increase in a manner that resembles the end of a run, with increases in both mean and root-mean-square levels. This behavior has not been seen before, and no good explanation is available. Again, disturbances originating downstream seem to propagate upstream within the subsonic part of the boundary layer.

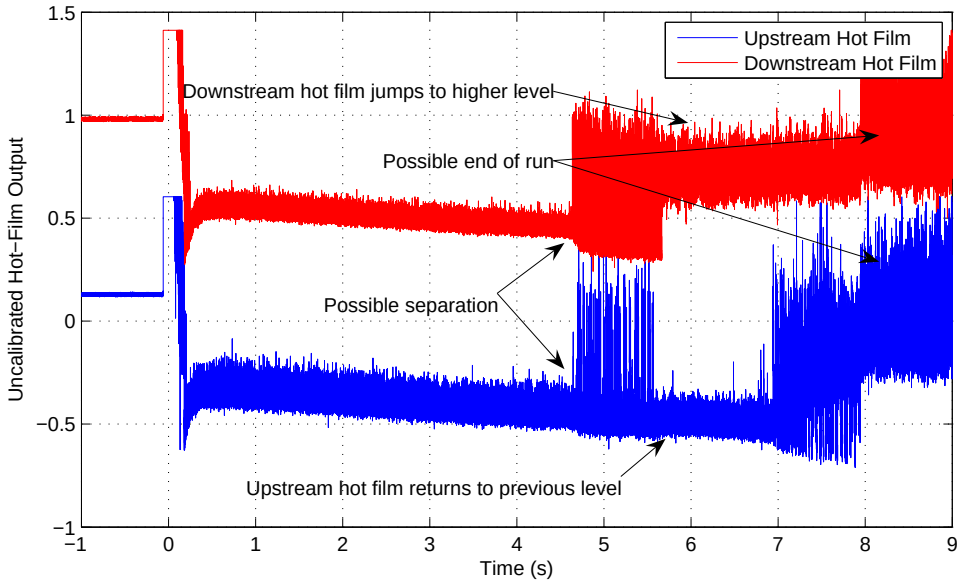

Figure 11: Wall-mounted hot films indicating asynchronous separation

IV.B.2. Empty Tunnel

Next, the cone model and sting were removed. The sting support was left in place. Bleeds-open runs were conducted for $p_{0i} = 140$ and 150 psia, at a time when the maximum quiet pressure was 143 psia. The run that started quiet indicated a 3.0 s run time and no separation. The run that started at 150 psia had only a 2.3 s run time and also did not separate. These runs were conducted shortly after the tunnel was accidentally run with the gate valve closed, and had very many turbulent bursts — 80–100 per second when starting quiet, 150–200 per second when starting noisy.

IV.B.3. Apollo Model

A 2-in.-diameter porous Apollo model at 24° angle of attack was tested in the BAM6QT at various pressures, orientations, and air blowing rates.[19] Unfortunately, the Apollo model seems to have caused separation of the nozzle-wall boundary layers during all runs, and the flow did not seem to start properly. Figure 12 shows hot-film traces for a typical run with the Apollo model as far forward as possible at $z = 2.31$ m. All runs at these conditions were characterized by a fluctuating voltage on the nozzle-wall hot films, with intermittent bursts. In these cases, the root-mean-square voltage of the nozzle-wall hot films is roughly the same as prior to the run, suggesting that the nozzle wall boundary layer is laminar. However, the oscillations and the general shape of the hot-film traces are abnormal. Later tests would show $M \approx 5.4$ when the hot films exhibited this behavior, suggesting that the boundary layer was separated and the tunnel did not start properly.

Several more runs were completed at higher initial stagnation pressures of 120 and 135 psia with the model at $z = 2.31$ m. These runs were performed with no blowing in order to see the effect of varying tunnel pressure. At these higher pressures, the hot film signals from the nozzle walls and model were dominated by strange 100 Hz oscillations, making it unclear if the tunnel had started. The model was rotated 90° and then 180° from its initial windward-side-down orientation, and the oscillations still occurred.

IV.C. Straight-Pipe Insert

IV.C.1. Slender Model

In early April, the straight pipe insert was installed with a 0.75-in. space between the leading edge of the insert and the 45° expansion adapter flange. Bleeds-open runs were conducted with a slender model in the

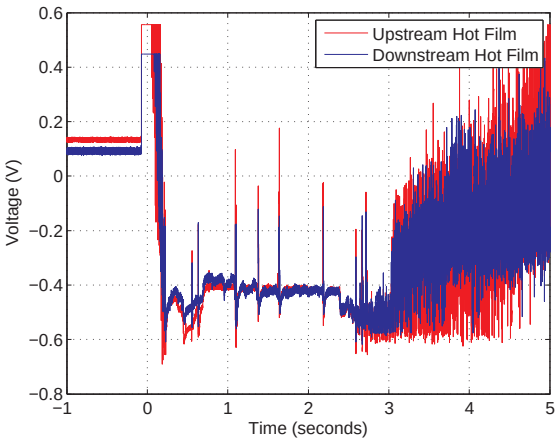

Figure 12: Wall hot films, Apollo model in new diffuser section with 9° ramp insert

tunnel for p_{0i} both above and below the maximum quiet pressure (90 psia). No separation was detected and the run time was 3.0 s for both cases.

IV.C.2. Apollo Model

Testing with the Apollo model was repeated after the straight pipe insert was installed in the sting support section to see if the model would start properly. The effect of model position on tunnel starting was also explored. When the model was positioned as far forward as possible, the hot film signals from the nozzle wall exhibited the same strange behavior as with the 9° nylon insert. When the model was positioned farther downstream, either at the streamwise location of the lip, or within the insert, the signals were again dominated by oscillations. Again, this was the same behavior observed with the nylon insert. This was also seen with the sphere-cone model discussed below.

IV.C.3. Sphere-Cone Model

A 2-in.-diameter, 70° sphere-cone was then placed in the tunnel under similar conditions as the Apollo model. The pipe insert was still installed in the tunnel. This model had a centerline Kulite pressure transducer and thus would normally measure total pressure behind a normal shock. Mach numbers were calculated directly from the stagnation pressure and should show $M = 6.0$ for a quiet run, and $M = 5.8$ for a noisy run. Two runs with the sphere-cone are shown in Figure 13. The first run was conducted with the model at $z = 2.36$ m. Earlier tests had demonstrated that this model would start with no sting-support section insert.[17] The wall hot-film traces were similar to Apollo model runs near that test section location. As before, the hot-film traces appear quiet, however the mean voltage is flat and does not have a small downward slope as is normally seen in quiet flow. There are also fluctuations in the mean voltage and some spikes within the traces. Also, the downstream hot film ($z = 2.07$ m) exhibits oscillations and bursts. The hot-film data were once again fairly ambiguous and did not show whether the flow was starting properly.

The Mach number was calculated using the mean stagnation point pressure at every 0.1 s throughout the runs. It was approximately Mach 5.6 during the quiet portion of the run. This is below the expected Mach 6 flow and strongly suggests the flow did not start properly. Reference 17 shows $M \approx 6.0$ for this sphere-cone model for a started and attached quiet run, and $M \approx 5.4$ for separated flow. Another run was conducted with the sphere-cone model placed at the upstream edge of the pipe insert ($z = 2.59$ m). The run was dominated by oscillations as was seen with the Apollo model in similar positions. Again, the Mach number calculated from the mean pitot pressure was approximately 5.6 during the run, which suggests the flow is not starting properly. Some separation of the nozzle wall boundary layer appears to occur, reducing the Mach number of the core flow.

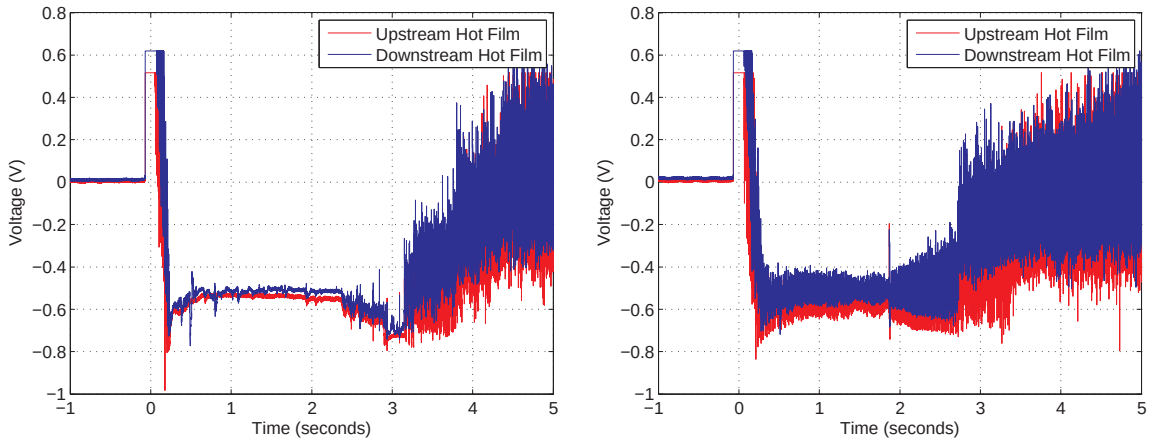

(a) Model at $z = 2.36$ m, P_0=90 psia (b) Model at $z = 2.59$ m

Figure 13: Wall hot films, sphere-cone model in new diffuser section with pipe insert

V. Far Downstream Observations of Low Pressure Fluctuations in the Diffuser

A Kulite model XCQ-062-15A pressure transducer was installed in the downstream end of the diffuser at $z = 5.00$ m downstream of the nozzle throat. It was mounted in the wall, but was not quite flush. There was a small cavity, about 0.1 in. deep, above the transducer. The calibrated output of the diffuser pressure transducer was compared to that of an uncalibrated hot film located on the nozzle wall at $z = 2.07$ m. The hot film and pressure transducer are offset azimuthally by 180°. These tests were conducted with the new sting support section and straight pipe insert installed.

Unexpectedly, the fluctuations in the diffuser transducer dropped dramatically when noise levels in the nozzle fell from conventional to quiet. Figure 14 shows the uncalibrated signal from the hot film along with the diffuser static pressure, the blue and red traces, respectively. Figure 14a is for an initial stagnation pressure of 124.4 psia. In this case, conventional noise levels were observed for the duration of the run. Figure 14b is for an initial stagnation pressure of 99.9 psia. This pressure is slightly below the maximum quiet pressure at the time of the experiments. Thus, the tunnel noise levels were low for the duration of the run. In both instances, a slender model and 1.5-in.-diameter sting were located in the nozzle exit. The initial stagnation temperature was 160 °C.

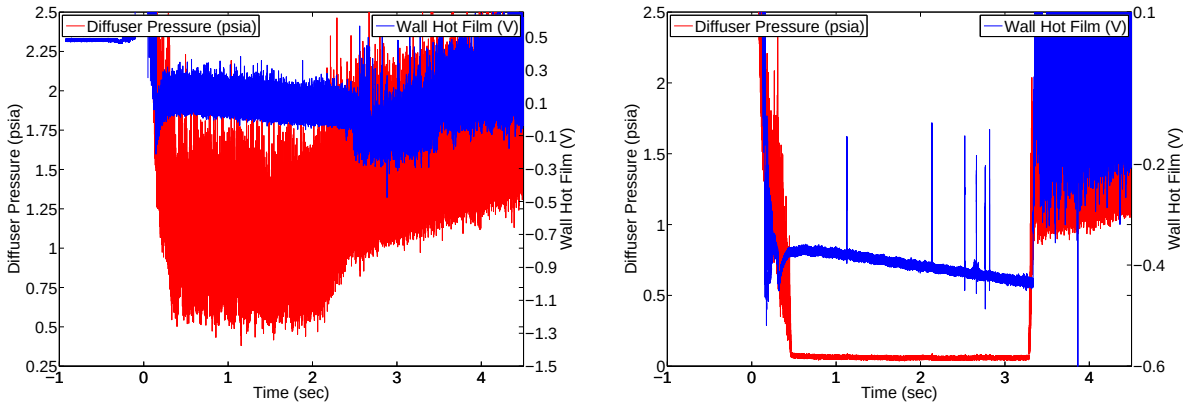

(a) Conventional noise levels (b) Reduced noise levels

Figure 14: Wall hot-film trace and diffuser static pressure

The RMS for both the wall hot film and the diffuser static pressure is significantly higher under conventional noise levels than for quiet freestream noise levels. The low RMS diffuser static pressure during quiet

flow suggests that the wall boundary layer may be laminar to the diffuser exit. This is very surprising.

Two runs were also made with an initial stagnation pressure of about 115 psia. Since the tunnel dropped to low noise levels at about 102 psia, the noise levels dropped from conventional to low levels during these runs. Figure 15 shows the diffuser static pressure, wall hot-film voltage trace, and the RMS of these signals. Red lines and symbols are the diffuser pressure while blue lines and symbols are for the wall hot film. The pressure RMS was nondimensionalized by the mean pressure during the time for which the RMS was calculated. Figures 15a and 15c are with the model and sting located near the exit of the test section while Figures 15b and 15d are for an empty tunnel. In Figures 15c and 15d, each point corresponds to the RMS calculated over a 50 ms period.

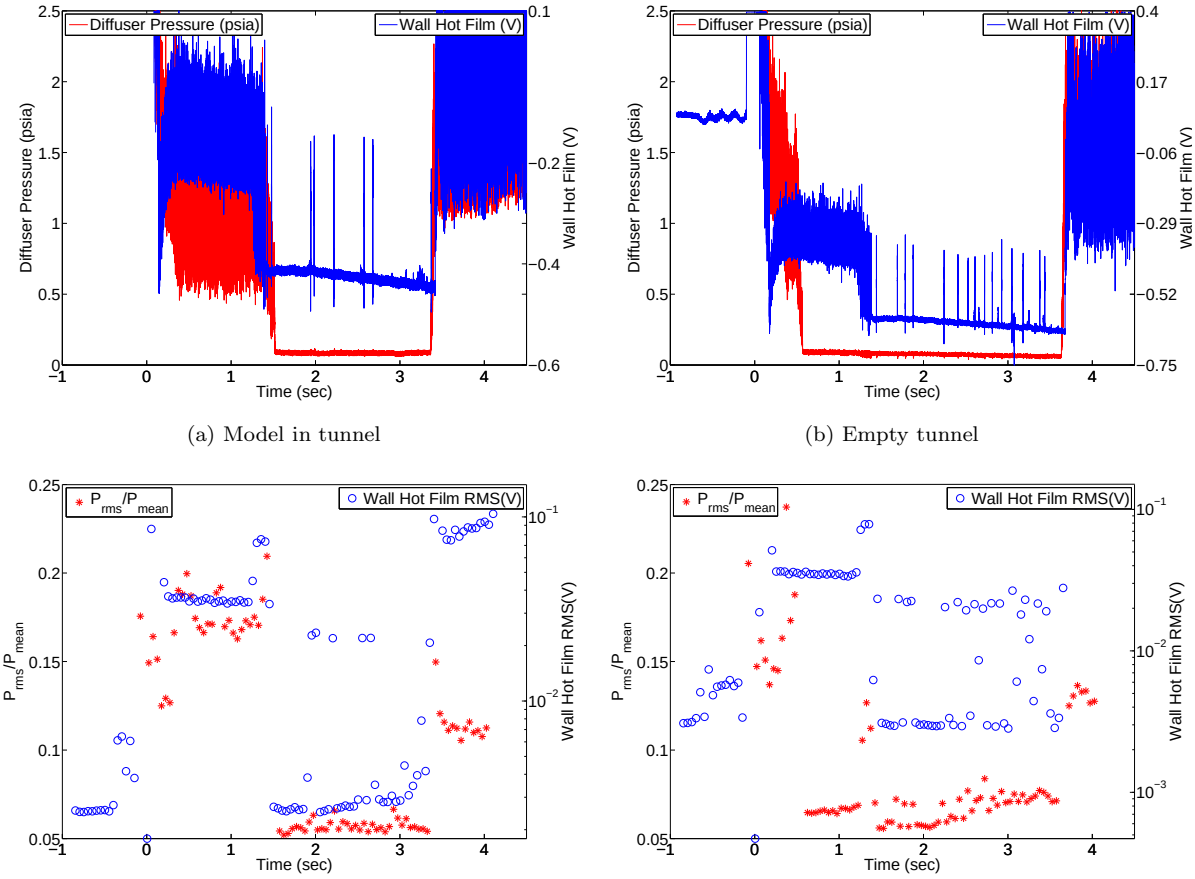

(a) Model in tunnel

(b) Empty tunnel

(c) RMS with model in tunnel

(d) RMS with empty tunnel

Figure 15: Wall hot-film trace and diffuser static pressure and RMS with and without model

In Figures 15a and 15c, both the hot-film and pressure-transducer signals show high RMS levels until about $t = 1.4$ s, when they drop by more than an order of magnitude. They remain low until the tunnel unstarts at about $t = 3.4$ s. The drop coincides with the drop in freestream noise level when the nozzle-wall boundary layer becomes laminar. Departures from low RMS levels are due to the passing of short-duration turbulent bursts, which can be seen in the mean traces. The RMS pressure transducer signal drops to a low value approximately 117 ms after the hot film and also shows the unstart approximately 55 ms earlier than the hot film. This means that the laminarization of the boundary layer traveled downstream at a speed of 2.08 m/s and that at the end of the run, the shock traveled upstream at a speed of 4.45 m/s. This behavior is not unexpected due to the pressure transducer being located so far downstream of the hot film.

Additionally, the pressure transducer does not clearly show the eight turbulent bursts evident in the hot-film trace. However, the RMS of the static pressure does generally increase slightly when the RMS of the hot-film signal spikes due to a passing turbulent burst. The relative timing of the drop in RMS for both the hot film and the pressure transducer strongly suggest that when the nozzle-wall boundary layer becomes laminar, it remains so to the end of the diffuser.

A substantial difference is noted when the model was removed, as shown in Figures 15b and 15d. The hot-film trace behaves the same way as in Figure 15a, starting with a high RMS and dropping to a much lower RMS when the nozzle-wall boundary layer becomes laminar. It appears from the hot-film trace that the boundary layer in the nozzle exit is turbulent from $t = 0$–1.4 s and laminar from $t = 1.4$ s until the tunnel unstarts at $t = 3.4$ s. The pressure transducer output does not show such a dramatic decrease in RMS when the tunnel noise levels drop. In fact, the pressure trace looks nearly identical to that shown in Figure 14b, a run that was entirely quiet. In Figure 15d, it is clear that the RMS does drop somewhat when the tunnel noise levels decrease at $t = 1.4$ s. In this case, the drop is only about 15%, much less than the order of magnitude drop observed in Figure 15c. Again, the RMS of the static pressure does generally increase slightly when the RMS of the hot film signal spikes due to a passing turbulent burst.

The relative timing of the apparent onset of a laminar boundary layer is surprising, especially considering that when a model was in the tunnel both signals dropped at nearly the same time. It is possible that a favorable pressure gradient at the aft end of the pipe insert causes the turbulent boundary layer to relaminarize by the time it reaches the pressure transducer. Reference 20 presents an extensive review of relaminarization. Residual fluctuations inherited from the turbulent boundary layer could account for the 15% higher pressure RMS observed before the entire nozzle-wall boundary layer appeared to became laminar at $t = 1.4$ s.

If a turbulent boundary layer in the empty tunnel relaminarizes, it seems clear that this does not happen when the model is in the tunnel. This would not be surprising. The model shock impinges at an unknown location on the nozzle-wall boundary layer. If it impinges on a relaminarized boundary layer, it is possible that the shock-induced adverse pressure gradient causes the boundary layer to retransition. Even if it impinges on the shear layer exiting the pipe insert or on the insert's boundary layer, it seems likely that it could disrupt the boundary layer flow enough to preclude relaminarization, even in the presence of the strong, favorable pressure gradient. It would be helpful to install several thin, surface-mounted hot films along the diffuser to better ascertain the behavior of the boundary layer there.

VI. LDI Development

The laser differential interferometer is a nonintrusive optical flow diagnostic device particularly applicable to low-density flow.[21–28] It measures the optical-path-length difference between two laser beams known as reference and signal beams. When the beams pass through a flow whose density fluctuates in time, causing its index of refraction to change, the optical path length of the beams varies and the difference in their individual variations is recorded by the LDI. Among the advantages of the LDI over other nonintrusive techniques are its high sensitivity, good spatial resolution, and large bandwidth.[29–33] Smeets and George developed the first version of the LDI in 1973, with which they were able to resolve optical path length differences as small as $\lambda/30,000$ over bandwidths between 100 Hz and 10 MHz.[22] Salyer developed a feedback-stabilized version of the LDI at Purdue University able to resolve minimum path length differences of $\lambda/13,000$ at a bandwidth of 6 MHz.[32,33] Salyer's LDI system was reassembled and improved by upgrading to a commercial balanced photodetector able to detect a minimum path-length difference of $\lambda/21,000$ at frequencies ranging from DC to 80 MHz (3 dB signal drop). Furthermore, the system was adapted to the BAM6QT with a vibration control system.

A schematic of the basic LDI setup is shown in Figure 16. The basic system works by sending two parallel laser beams through the flow which are later reunited to a single beam. This beam is then split into two beams with complementary interference patterns. The two resulting beams are focused onto a pair of photodiodes whose currents are subtracted and difference recorded. Note that Figure 16 was based on the LDI schematic reported by Salyer. See Ref. 34 for further details on the performance of each optical element and the theory behind the LDI.

A New-Focus Model 1807-FS Balanced Photodiode Receiver was used as the photodetector for the LDI. This was an upgrade from the home-built photoreceivers that Salyer used for his research in the Purdue Quiet Flow Ludwieg Tube (PQFLT).[30–33] The function of this receiver is to subtract the photocurrent generated by the two photodiodes. By doing this, common-mode-noise (such as laser-intensity noise) that is present on both the reference and signal beams is canceled out and suppressed from the signal. In addition, a signal twice as large in amplitude is obtained. The frequency response of the photoreceiver has a drop of 3.0 dB between 80 MHz and about 100 MHz.[35]

Measurements of the noise in the LDI signal were made with the vibration control system. Figure 17a

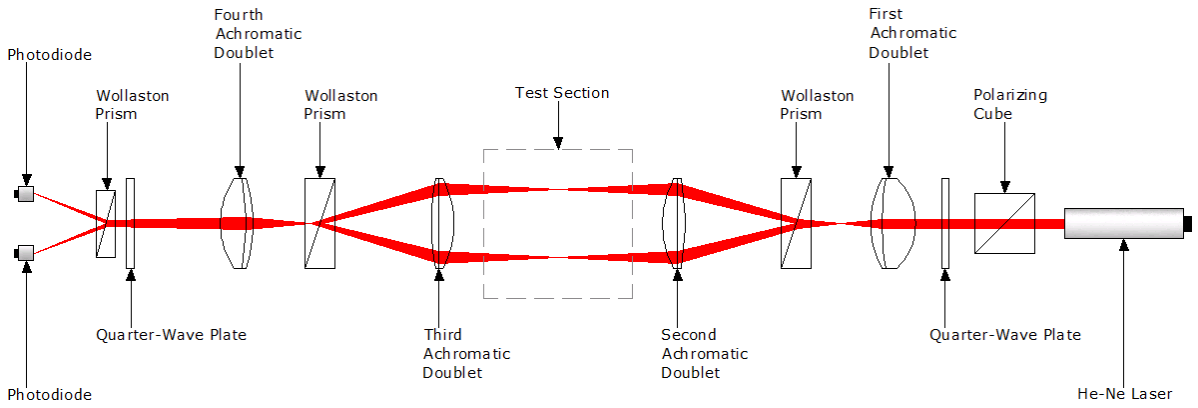

Figure 16: Schematic of basic LDI

shows a 0.2 s LDI calibrated optical-path-difference output signal, sampled at 1 MHz, while both beams were passing through stagnant room air. To estimate the peak-to-peak amplitude of the noise, the very low frequencies were canceled by subtracting from the data a running average with a window size equal to 1% of the number of data points in the set as shown in Figure 17b. The power spectrum of the noise is shown in Figure 17c. Note the large-amplitude, low-frequency noise in the signal. Mechanical vibrations in the room or in the optical mounts are likely the primary source of this noise. It has a pronounced resonant frequency of about 425 Hz with an amplitude of approximately $2 \cdot 10^3$ nm^2/Hz. A closer look was taken at similar data and the high-frequency noise was analyzed. The instabilities that the LDI is intended to detect are at much higher frequencies ($\approx$ 100 kHz) than these mechanical vibrations. Thus, the minimum optical path length difference detectable by the LDI, for the purposes of this research, is determined by the peak-to-peak amplitude of this high-frequency noise.

Figure 18b shows a 1-ms calibrated set of filtered LDI data, sampled at 1 MHz (filtered in the same fashion as the low-frequency noise data). Hence, the LDI assembled in the BAM6QT with vibration control has a minimum detectable optical path length difference of approximately $\lambda/21,000$, obtained by dividing the amplitude of the noise by λ.

The root-mean-square (RMS) of the noise was 0.39 mV. This is an improvement from Salyer's active photodiode receiver capable of detecting optical path length differences as small as $\lambda/13,000$ with a noise RMS value of 0.84 mV (Ref. 32 pg. 42). Note, however, that Salyer used alternating high-performance LED lamps to measure the bandwidth of the system and the peak-to-peak amplitude of the electrical noise rather than the signal of the feedback-stabilized LDI. Although it would be expected that more sources of noise affect the signal of the feedback-stabilized LDI than those that affect the signal from a pair of alternating LED lamps shining on the photoreceiver, the sampling frequencies are not the same and the data obtained from each are not precisely comparable. Further specifications on the feedback stabilization system are reported in Refs. 32 and 34.

VII. Forward-Facing Cavity Measurements Under Quiet Flow

A forward-facing cavity is simply a hemisphere with a circular hole drilled in its center. The model used in this experiment, shown in Figure 19, had an adjustable cavity depth L from 0 to 3 times the cavity diameter D. All the forward-facing cavity studies were performed in the Purdue Quiet-Flow Ludwieg Tube (PQFLT) at Mach 4. The forward-facing cavity can be regarded as a resonance tube. Engblom et al. numerically simulated the unsteady flow inside the cavity and obtained agreement with the experimental data for the pressure oscillations at the base of the cavity.[36] Using their experimental and computational results, Hoffman et al. state that the frequency of the oscillations is inversely proportional to the cavity depth and the amplitude is directly proportional to it.[37] Ladoon et al. measured pressure fluctuations inside a forward-facing cavity and found primary mode frequencies and harmonics for cavity depth ratios (L/D) ranging from 0.0 to 1.984. They stated that "the cavity was found to be very sensitive to freestream noise. Even very weak freestream disturbances that are normally too small to be detected are amplified to measurable levels by the cavity".[38] Kim and Park also reported that perturbations in the freestream excited

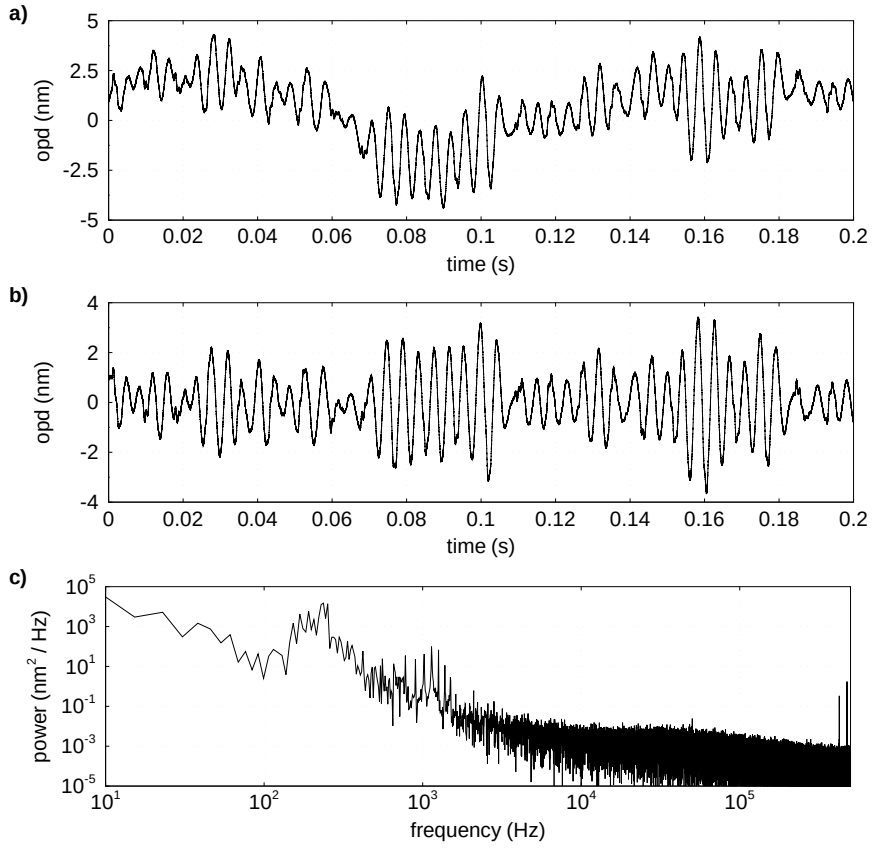

Figure 17: LDI mechanical noise due to vibrations in the BAM6QT laboratory: a) raw noise trace, b) raw signal minus running average, c) noise power spectrum

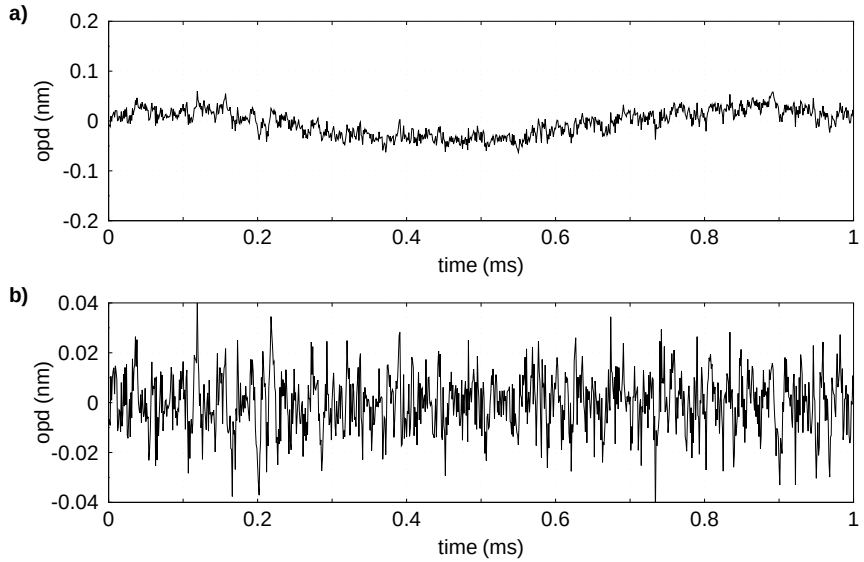

Figure 18: LDI electrical noise in the BAM6QT: a) raw noise trace, b) raw signal minus running average

the oscillations inside the cavity at the acoustic resonant frequency for various L/D values.[39] Engblom et al. confirm that fluctuations inside the cavity resonate at the primary mode ('Organ-Pipe') frequency which is inversely proportional to cavity depth. They also mention that the amplification of the fluctuations by the cavity is thought to be directly proportional to the cavity depth.[40,41] Lastly, they reported that numerical results predict unstable deeper cavities which resonate strongly without freestream noise, generating self-sustained resonant oscillations.[40] However, Ladoon et al. state that that these deep-cavity simulations have not been experimentally confirmed in a quiet-flow facility.[38] Further numerical results on forward-facing cavity flow are found in Refs. 36 and 42.

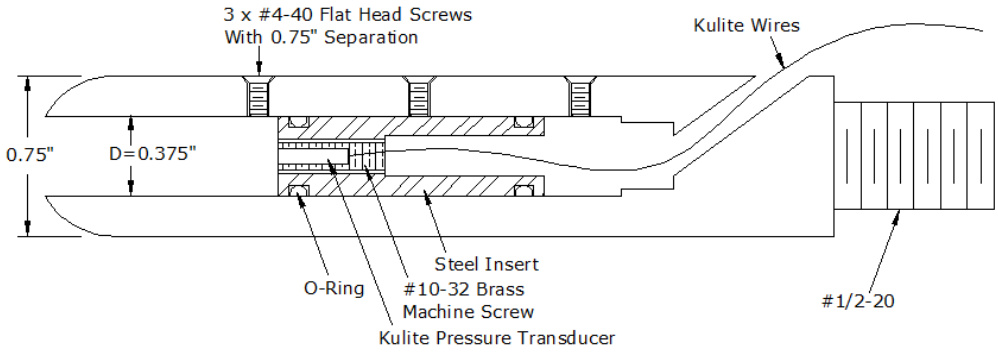

Figure 19: Forward-facing cavity model tested in the PQFLT

Figures 20 and 21, reproduced from Ref. 34, show the levels of freestream noise in the test section of the PQFLT during 12 individual runs along with the mean Mach number as it varies during a run. The legend refers to the initial driver pressure for each run. The tunnel is running quietly for $p_0 < 11$ psia with a Mach number near 4.0.

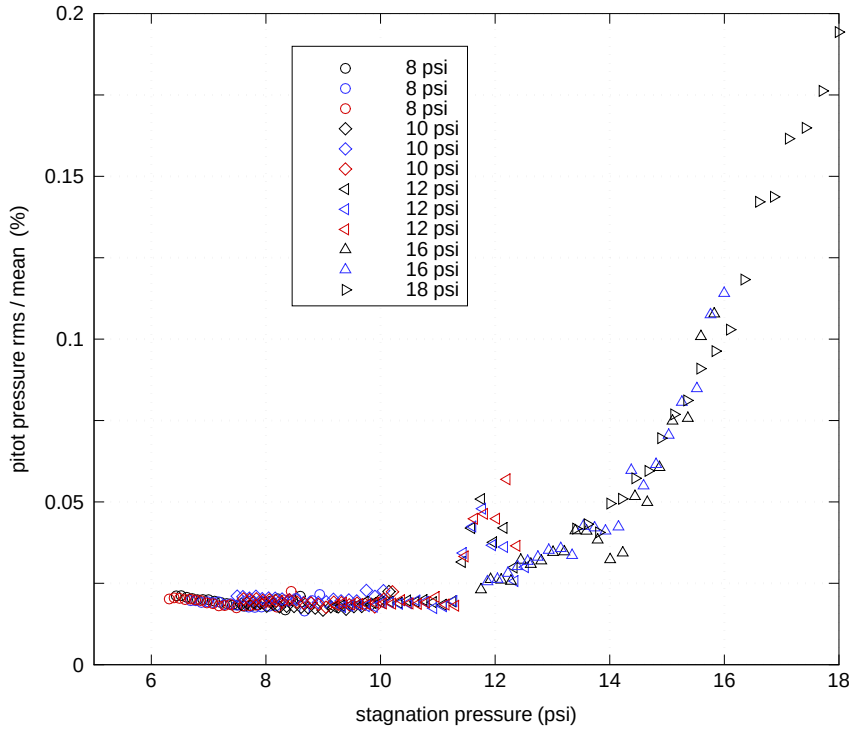

Figure 20: Freestream noise level in the PQFLT measured with 0.067 in.-diameter pitot probe

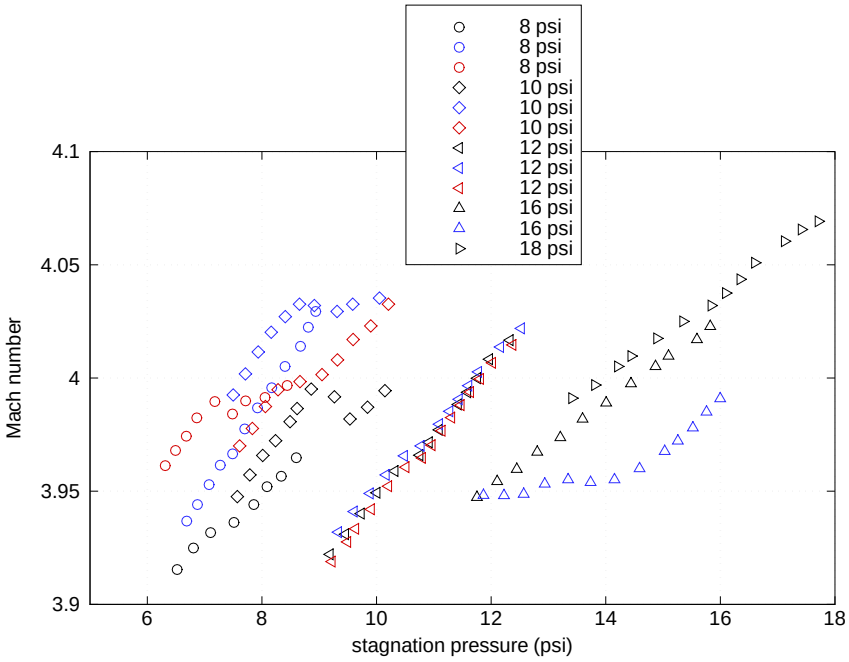

Figure 21: Mach number inside the PQFLT test section.

Figure 22 shows the power spectra of the pressure signal during a tunnel run at the base of the forward-facing cavity, obtained with a flush-mounted Kulite pressure transducer, at various cavity depths. Note that primary mode frequency peaks for the shallower cavities are broader than the peaks for the deeper cavities. Higher-mode peak frequencies occur at integer multiples of the primary mode, as expected.

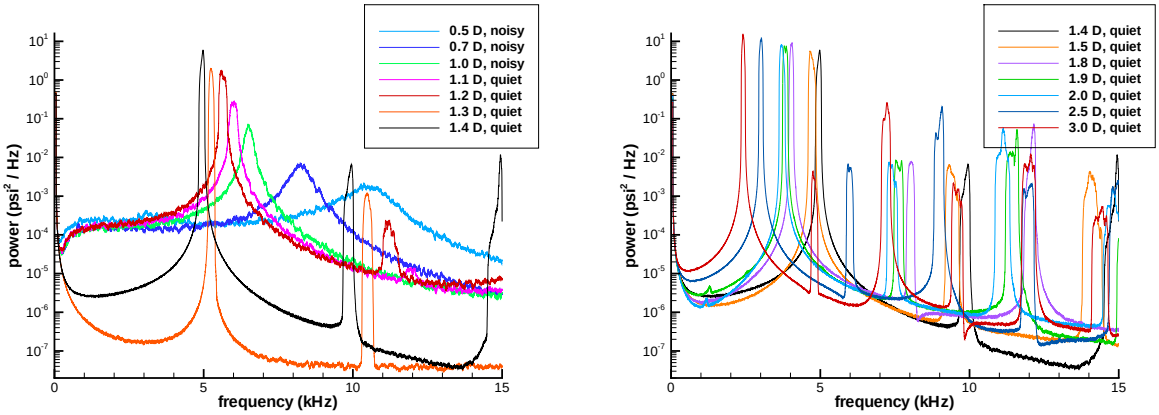

(a) $L/D \leq 1.4$ (b) $L/D \geq 1.4$

Figure 22: Kulite power spectra for forward-facing cavity of various depths

Figure 23 shows the experimental primary mode resonant frequency and amplitude as a function of cavity depth along with the theoretical 'organ-pipe' frequency f given by

$$\omega = 2\pi f = \pi \frac{D}{2L^\star}, \tag{1}$$

where

$$L^\star = L + \delta, \tag{2}$$

is the distance from the cavity base to the mean shock position.[38] The bow shock standoff distance δ, was obtained from Figure 4.15 in Ref. 43, since it is not known for a forward-facing cavity. An approximation of $\delta/d = 0.24$ was chosen between the value for a 3-dimensional cylinder with a flat nose, and a sphere. Note that the points plotted in Figure 23 are only for the primary mode frequency peaks displayed in Figure 22 and not for any of the harmonics also displayed in the plot. The amplitude of the peaks was obtained by integrating the frequency peaks between frequencies where the amplitude dropped by a factor of ten from the peak amplitude.

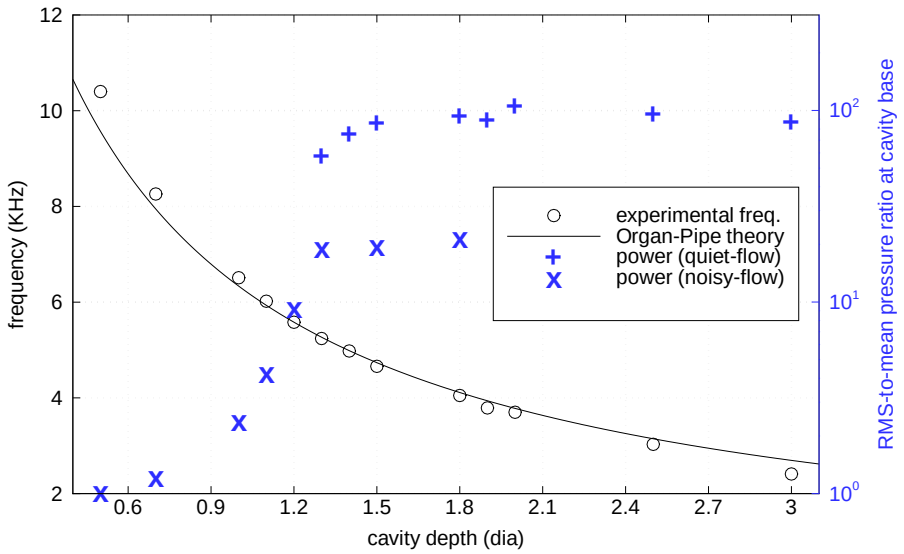

Figure 23: Primary mode resonant frequency and amplitude as a function of cavity depth

Power spectra of the Kulite data are displayed in Figure 24 for quiet ($p_{0i} = 8$ psi) and noisy ($p_{0i} = 24$ psi) runs at several low cavity depths ranging from 0.5 D to 1.2 D. Note that at a cavity depth of 0.5 D the cavity resonates in quiet flow. This is a repeatable phenomenon but the cause is unknown. For other depths less than 1.2 D the cavity does not display any pronounced resonance under quiet flow. However, a small peak can be observed in the spectra of quiet runs at depths of 1.0 D, 1.1 D, and 1.2 D. The small peak happens at the same dominant frequency of the freestream disturbance resonance of the cavity in noisy flow. This indicates that the forward-facing cavity also works as a mechanical amplifier of low-amplitude freestream disturbances present in quiet flow that are not detectable with other instrumentation such as hot-wires, hot-films, or pressure transducers. On the other hand, for depths of 1.3 D and above, the cavity self-resonates even in quiet-flow and a clear ringing frequency for several cavity depths ranging from 1.3 D to 3.0 D can be observed in Figure 25 during runs with $p_{0i} = 8$ psi. The amplitudes of the primary resonant frequencies of runs made under noisy conditions at depths of 1.3 D, 1.5 D, and 1.8 D are plotted in Figure 23. The amplitude of the primary resonant frequency does not vary much with freestream noise when the cavity is deeper than 1.2 D. This is the first experimental confirmation of Ladoon et al.'s prediction of a forward-facing-cavity critical depth beyond which the cavity self-resonates independently of freestream noise.

VIII. Conclusion

The BAM6QT continues to provide quiet flow for stagnation pressures up to 120–140 psia. Controlling scratches and dust in the nozzle throat remains critical to maintaining performance.

With the original straight sting-support section, a 2.5-in.-diam. 70° sphere-cone model could be started during quiet runs. Surprisingly, under noisy flow with turbulent nozzle-wall boundary layers, a similar 2.0-in.-diam. model barely starts, perhaps because the turbulent boundary layer is thicker. A 2.0-in.-diam. porous Apollo model was built to study blowing effects, but failed to start at 24° angle of attack. Since a 7° sharp cone can be started with a 5.5-in. base diameter, this is presumably due to shock/boundary-layer

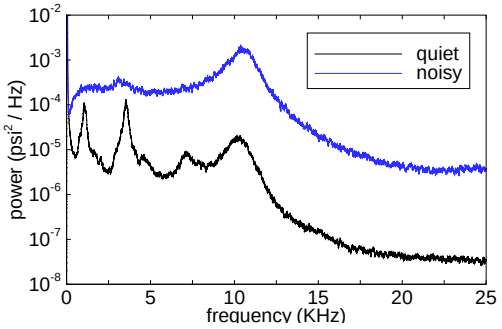

(a) Cavity depth $\frac{L}{D} = 0.5$

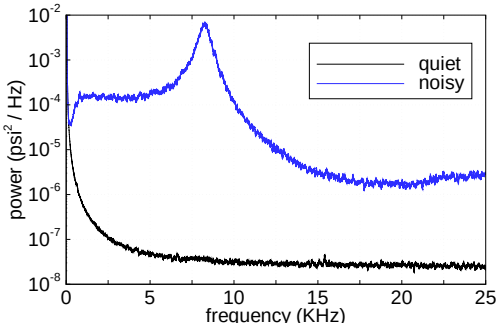

(b) Cavity depth $\frac{L}{D} = 0.7$

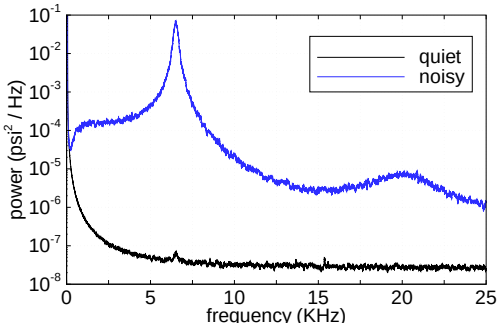

(c) Cavity depth $\frac{L}{D} = 1.0$

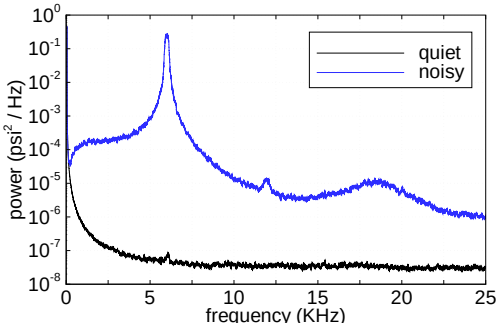

(d) Cavity depth $\frac{L}{D} = 1.1$

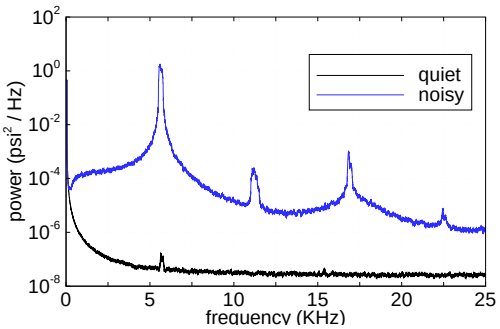

(e) Cavity depth $\frac{L}{D} = 1.2$

Figure 24: Power spectra of forward-facing cavity Kulite

interactions on the nozzle walls. New sting-support and diffuser sections were installed to increase the tunnel diameter from 9.5 to 14.1 in. aft of the nozzle. Two inserts have been installed downstream of the nozzle in an effort to control the shock/boundary-layer interactions and start larger models with stronger bow shocks. These efforts have been unsuccessful so far. Instead, the tunnel run time has been reduced from 6–8 to 3–5 s.

A pressure transducer was installed near the end of the new diffuser. Surprisingly, this indicated that quiet flow was sometimes observed far downstream of the nozzle exit.

The laser differential interferometer has been rebuilt for the BAM6QT. Preliminary tests show a minimum detectable optical path length difference of approximately $\lambda/21,000$, with increased bandwidth.

Resonance in forward-facing cavities was measured in the Mach-4 tunnel under quiet and noisy flow. Resonant frequencies matched the theoretical organ-pipe prediction. Predictions of self-resonance for deep cavities were confirmed, although the critical length-to-diameter ratio that was predicted is considerably higher than the one observed. Small primary-mode pressure fluctuations are detected at the cavity base even under quiet flow, for shallow cavities approaching the critical length-to-diameter ratio. This suggests that a forward-facing cavity with a depth of approximately 1.2 diam. may be used as a mechanical amplifier of small-amplitude freestream disturbances.

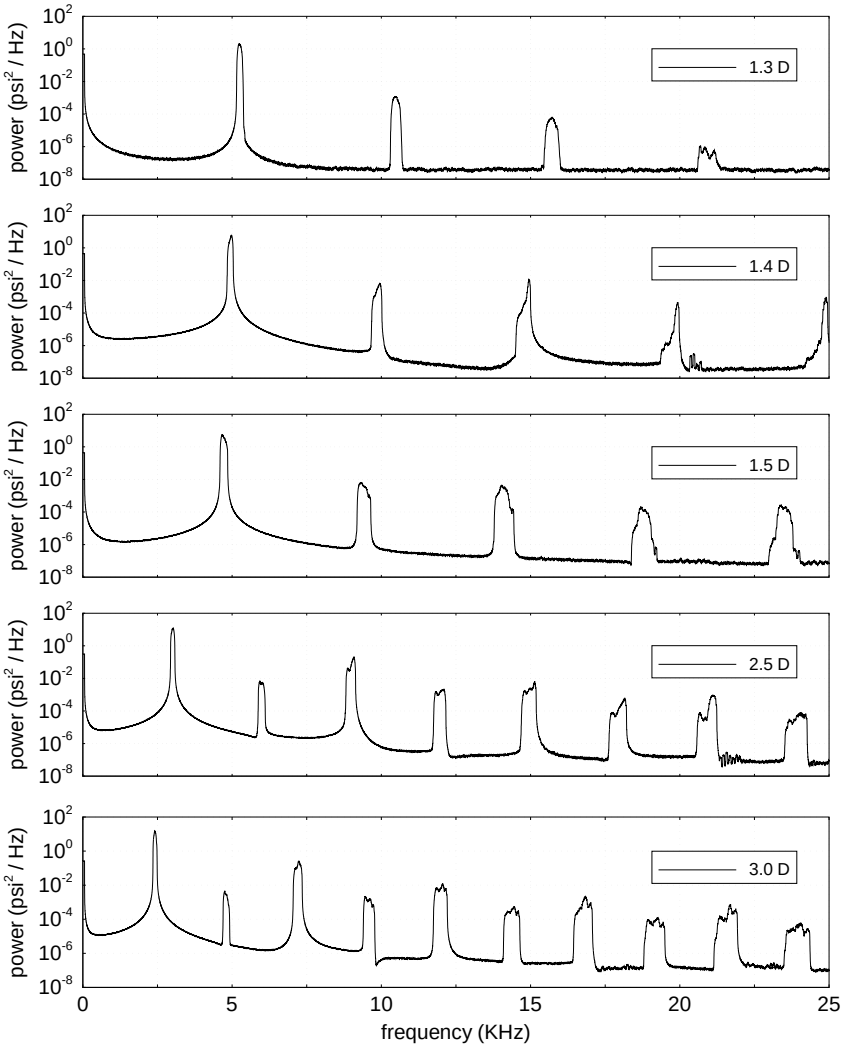

Figure 25: Power spectra of self-oscillating forward-facing cavity Kulite data at various depths in quiet flow

Acknowledgments

Research in the quiet tunnels is funded by AFOSR under grant FA9550-06-1-0182, by NASA under the Fundamental Aeronautics and Constellation University Institute programs, and by Sandia National Laboratory. Katya Casper was funded by a National Defense Science and Engineering Graduate Fellowship. Detailed design and fabrication of the new diffuser and sting-support sections was carried out by Lagrange Products of Lagrange, Indiana (ASME Pressure Vessel design and manufacturing), Anderson Tool and Engineering of Anderson, Indiana (detailed design and machining), and ATK/Microcraft of Tullahoma, Tennessee (turning of the long internal taper within the diffuser).

References

[1]Steven P. Schneider. Laminar-turbulent transition on reentry capsules and planetary probes. *Journal of Spacecraft and Rockets*, 43(6):1153–1173, November–December 2006.

[2]Steven P. Schneider. Hypersonic laminar-turbulent transition on circular cones and scramjet forebodies. *Progress in Aerospace Sciences*, 40(1-2):1–50, February 2004.

[3]I. E. Beckwith and C. G. Miller III. Aerothermodynamics and transition in high-speed wind tunnels at NASA Langley. *Annual Review of Fluid Mechanics*, 22:419–439, 1990.

[4]Steven P. Schneider. Effects of high-speed tunnel noise on laminar-turbulent transition. *Journal of Spacecraft and Rockets*, 38(3):323–333, May–June 2001.

[5]Steven P. Schneider. Flight data for boundary-layer transition at hypersonic and supersonic speeds. *Journal of Spacecraft and Rockets*, 36(1):8–20, January-February 1999.

[6]S. P. Wilkinson, S. G. Anders, and F.-J. Chen. Status of Langley quiet flow facility developments. Paper 94-2498, AIAA, June 1994.

[7]I. Beckwith, T. Creel, F. Chen, and J. Kendall. Freestream noise and transition measurements on a cone in a Mach-3.5 pilot low-disturbance tunnel. Technical Paper 2180, NASA, September 1983.

[8]A. E. Blanchard, J. T. Lachowicz, and S. P. Wilkinson. NASA Langley Mach 6 quiet wind-tunnel performance. *AIAA Journal*, 35(1):23–28, January 1997.

[9]S. P. Schneider. The development of hypersonic quiet tunnels. AIAA Paper 2007-4486, June 2007. Revised version to appear in Journal of Spacecraft and Rockets.

[10]I. E. Beckwith, W. D. Harvey, J. E. Harris, and B. B. Holley. Control of supersonic wind-tunnel noise by laminarization of nozzle-wall boundary layers. Technical Report TM X-2879, NASA Langley Research Center, Hampton, VA 23665, December 1973.

[11]W. D. Harvey, P. C. Stainback, J. B. Anders, and A. M. Cary. Nozzle wall boundary-layer transition and freestream disturbances at Mach 5. *AIAA Journal*, 13(3):307–314, March 1975.

[12]Steven P. Schneider. Design and fabrication of a 9.5-inch Mach-6 quiet-flow Ludwieg tube. AIAA Paper 1998-2511, June 1998.

[13]B. H. Carmichael. Summary of past experience in natural laminar flow and experimental program for resilient leading edge. NASA Contractor Report 152276, May 1979.

[14]T. J. Juliano, E. O. Swanson, and S. P. Schneider. Transition research and improved performance in the Boeing/AFOSR Mach-6 quiet tunnel. AIAA Paper 2007-0535, January 2007.

[15]S. P. Schneider and T. J. Juliano. Laminar-turbulent transition measurements in the Boeing/AFOSR Mach-6 Quiet Tunnel. AIAA Paper 2007-4489, June 2007.

[16]M. P. Borg, S. P. Schneider, and T. J. Juliano. Effect of freestream noise on roughness-induced transition for the X-51A forebody. AIAA Paper 2008-0592, January 2008.

[17]Michael J. Hannon, Jr. Evaluation of diffuser modifications for the Boeing/AFOSR Mach-6 Quiet Tunnel. Master's thesis, School of Aeronautics and Astronautics, Purdue University, August 2008.

[18]Thomas J. Juliano. Nozzle modifications for high-Reynolds-number quiet flow in the Boeing/AFOSR Mach-6 quiet tunnel. Master's thesis, Purdue University, School of Aeronautics and Astronautics, December 2006. Available from DTIC as ADA456772.

[19]K. Casper, J. Rubal, and B. Wheaton. Simulation of ablation on a porous Apollo model and its effect on laminar-turbulent transition. AAE 520 Final Project Report, May 2008.

[20]R. Narasimha and K.R. Sreenivasan. Relaminarization of fluid flows. *Advances in Applied Mechanics*, 19:221–309, 1979.

[21]G. Smeets and A. George. Gas-dynamic investigations in a shock tube using a highly sensitive interferometer. French-German Research Institute (ISL) Technical Report R 14/71. Translated by Andreas R. Goetz, June 1971. DTIC ADA307743.

[22]G. Smeets and A. George. Laser-differential interferometer applications in gas dynamics. French-German Research Institute (ISL) Technical Report R 28/73. Translated by Andreas R. Goetz, November 1973. DTIC ADA307459.

[23]G. Smeets and A. George. Investigation of shock boundary layers with a laser interferometer. *Stanford University Press, Stanford, California. Recent Development in Shock Tube Research*, pages 429–438, 1973. D. Bershader and W. Griffith, editors.

[24]G. Smeets. Density profiles of a subsonic free jet (d=80 mm), measured using the laser-differential interferometer. French-German Research Institute (ISL) Technical Note N 620/75. Translated by Andreas R. Goetz, November 1975. DTIC ADA307509.

[25]G. Smeets and A. George. Laser-interferometer with phase compensation. French-German Research Institute (ISL) Technical Report R 28/73. Translated by Andreas R. Goetz, December 1975. DTIC ADA307458.

[26]G. Smeets. Flow diagnostics by laser interferometry. *IEEE Transactions on Aerospace and Electronic Systems*, 13(2):82–90, March 1977.

[27]G. Smeets. Interferometry. French-German Research Institute (ISL) Technical Report CO 214/90, May-June 1990.

[28]G. Smeets. Interferometry in rarefied gas flows. French-German Research Institute (ISL) Technical Report CO 207/92, April 1992.

[29]S. H. Collicott, S. P. Schneider, and N. L. Messersmith. Review of optical diagnostic methods for hypersonic low-noise facilities. AIAA Paper 1996-0851, January 1996.

[30]T. R. Salyer, L. A. Randall, S. H. Collicott, and S. P. Schneider. Use of laser differential interferometry to study receptivity on a hemispherical nose at Mach 4. AIAA Paper 1998-0238, January 1998.

[31]T. R. Salyer, S. H. Collicott, and S. P. Schneider. Feedback stabilized laser differential interferometry for supersonic blunt body receptivity experiments. AIAA Paper 2000-0416, January 2000.

[32]T. R. Salyer. *Laser Differential Interferometry for Supersonic Blunt Body Receptivity Experiments*. PhD thesis, Purdue University School of Aeronautics & Astronautics, May 2002.

[33]T. R. Salyer, S. H. Collicott, and S. P. Schneider. Characterizing laser-generated hot spots for receptivity experiments. *AIAA Journal*, 44(12):2871–2878, December 2006.

[34]R. Segura. Oscillations in a forward-facing cavity measured using laser-differential interferometry in a hypersonic quiet tunnel. Master's thesis, Purdue University, School of Aeronautics & Astronautics, December 2007.

[35]New Focus Inc. 80-mhz balanced photoreceivers model 18x7 user's guide, 2003. Document Number 181710 Rev. A.

[36]W. A. Engblom, B. Yuceil, D. B. Goldstein, and D. S. Dolling. Experimental and numerical study of hypersonic forward-facing cavity flow. *Journal of Spacecraft and Rockets*, 33(3):353–359, May-June 1996.

[37]K. A. Hoffmann, Y. B. Suzen, and M. Papadakis. Numerical simulation of viscous flow for hypervelocity projectiles and interceptors with nose cavity. AIAA Paper 94-0213, January 1994.

[38]D. W. Ladoon, S. P. Schneider, and J. D. Schmisseur. Physics of resonance in a supersonic forward-facing cavity. *Journal of Spacecraft and Rockets*, 35(5):626–632, September-October 1998.

[39]J. D. Kim and S. O. Park. Unsteady characteristics of hypersonic forward facing cavity flow. AIAA Paper 2000-3925, 2000.

[40]W. A. Engblom, D. B. Goldstein, D. Ladoon, and S. P. Schneider. Fluid dynamics of hypersonic forward-facing cavity flow. AIAA Paper 96-0667, January 1996.

[41]W. A. Engblom, B. Yuceil, D. B. Goldstein, and D. S. Dolling. Hypersonic forward-facing cavity flow: An experimental and numerical study. AIAA Paper 95-0293, January 1995.

[42]S. I. Silton and D. B. Goldstein. Use of an axial nose-tip cavity for delaying ablation onset in hypersonic flow. *Journal of Fluid Mechanics*, 528:297–321, 2005.

[43]H. W. Liepmann and A. Roshko. *Elements of Gasdynamics*, chapter 4-14, Detached Shocks. John Wiley & Sons Inc., 1st edition, 1957.